TECHNISCHE UNIVERSITÄT DRESDEN

Validation of the background estimation in measurements of photon-induced WW production using $pp \rightarrow WZ$ events

Bachelor-Arbeit
zur Erlangung des Hochschulgrades
Bachelor of Science
im Bachelor-Studiengang Physik

vorgelegt von

Amalia Beer
geboren am 24.04.2000 in Radebeul

Institut für Kern- und Teilchenphysik
Fakultät Physik
Bereich Mathematik und Naturwissenschaften
Technische Universität Dresden
2024

Eingereicht am 9. Dezember 2024

1. Gutachter: Dr. Frank Siegert
2. Gutachter: Prof. Dr. Arno Strässner

Abstract

English:

The investigation of the self-coupling of electroweak gauge bosons opens up a broad field of possibilities to confirm predictions of the Standard Model and its underlying gauge theory. At the same time, precise analyses of such processes create the potential to discover deviations from well known physics. One of these processes is the $\gamma\gamma \to WW$ process, which proceeds via quartic and trilinear self-coupling of photons and W bosons. In the evaluation of experimental findings from the ATLAS detector at the LHC (CERN), the precise determination of the $q\bar{q} \to WW$ background is a particular challenge. In this work, the $q\bar{q} \to WW$ background estimation from the $\gamma\gamma \to WW$ analysis performed by the ATLAS Collaboration based on a Drell-Yan correction, is validated. For this purpose, a selection of events of the $q\bar{q} \to WZ$ process is performed and then compared to the reweighted theory-based event samples from the Monte Carlo simulation POWHEG+HERWIG7. Thus, a good match of this correction with high purity selected WZ events is shown.

Deutsch:

Die Untersuchung der Selbstkopplung von elektroschwachen Eichbosonen eröffnet ein breites Feld an Möglichkeiten zur Bestätigung von Vorhersagen des Standard Modells und dessen zugrundeliegender Eichtheorie. Gleichzeitig schaffen genaue Analysen solcher Prozesse das Potential, Abweichungen von bekannter Physik festzustellen. Einer dieser Prozesse ist der über vierfache und trilineare Selbstkopplung von Photonen und W-Bosonen vollzogene $\gamma\gamma \to WW$ Prozess. In der Auswertung experimenteller Befunde des ATLAS Detektors am LHC (CERN) ist die genaue Ermittlung des durch Fragmentierung des Protons entstehenden $q\bar{q} \to WW$ Untergrundes eine besondere Herausforderung. In dieser Arbeit wird die $q\bar{q} \to WW$ Untergrundabschätzung aus der von der ATLAS Collaboration durchgeführten $\gamma\gamma \to WW$ Analyse anhand einer Drell-Yan Anpassung validiert. Dafür wird eine Selektion des $q\bar{q} \to WZ$ Prozesses durchgeführt und mit dieser korrigierten Theorievorhersage der Monte-Carlo Simulation POWHEG+HERWIG7 für diesen Prozess verglichen. So konnte eine gute Übereinstimmung der Anpassung mit hoher Reinheit selektierter WZ Events gezeigt werden.

Contents

1 Introduction

With progressive development of the theoretical and experimental framework for the research in modern particle physics, the experimental analysis of processes potentially providing incongruities with the Standard Model is one of the most important aspects for future developments. Exploring every possible gap in a system we know is not complete builds the foundation for new ideas and theories that might bring humanity one step closer to fully understand our universe.

Since the the electroweak interaction force has been predicted and experimentally verified in the 1960s and 70s, many theoretically derived processes involving W and Z interaction bosons have been observed under global efforts in facilities like CERN, Fermilab and DESY. Further, many simulation models based on existing theoretical fundamentals have been introduced to compare with measured data from these research institutions.

An occurrence predicted by developments of the Standard Model and proven at the Large Hadron Collider at CERN is the elastic $\gamma\gamma \rightarrow WW$ process [1, 2]. In proton proton (pp) collisions, the high acceleration of electrically charged particles leads to an electromagnetic field in the transverse plane. Equivalently, this area is source of high energy virtual photons which can form a pair of massive and oppositely charged W bosons. This process proceeds through trilinear and quartic gauge-boson interactions is especially interesting as it only involves Feynman diagrams with self coupling of electroweak gauge bosons and therefore directly probes the theoretical SU(2)×U(1) gauge structure of the Standard Model [3].

For a detailed analysis of this process, an understanding of the background processes that disrupt the evaluation of the measurement is essential. These result mainly from the inelastic pp collisions and dissociation of the proton, which leads to a broad spectrum of decay products dominated by $qq \rightarrow WW$ processes. The estimation of these background events is difficult and as simulation of $\gamma\gamma \rightarrow WW$ is not yet fully available and models do not agree well in signal region and carry large uncertainties, the distinction between background and signal is essential.

Therefore, the development of a method for the estimation of $qq \rightarrow WW$ background is necessary. This work will provide a control region for a similar process, $qq \rightarrow WZ \rightarrow \ell\nu_\ell\ell^+\ell^-$, to validate the estimation for the $qq \rightarrow W^+W^- \rightarrow \ell^+\nu_\ell\ell^-\overline{\nu}_\ell$ background done in the Ref. [4] analysis. As the selection of three charged leptons is quite unique, it is expected to be more pure. For this purpose, a three lepton selection will be applied and different variables will be evaluated. Chapter 2 outlines the theoretical foundation for this analysis and gives a brief introduction to the Standard Model, especially to the relevant processes and how they are detected, reconstructed an analyzed. Chapter 3 is going to be dedicated to the selection and analysis, whereby the proceeding and results will be presented. The final Chapter 4 will provide a summary of the results and an outlook for the future.

2 Theoretical foundation

As the human species evolved from seemingly simple cell bunches to more and more complex creatures as we consider ourselves today, individuals started to ask more and more complex questions. What might have started as "Does rock consist of many rocks or is rock just rock?" ended up in a fundamental debate about the basic components the universe is made of.

When Democritus postulated the existence of the smallest indivisible units, the atoms, in 400 BC, he created the foundation for a scientific consensus that lasted 2300 years. It was only around 1900 that the more intensive search for the parts that make up atoms themselves began, which led to an avalanche of discoveries that continued until the middle of the 20th century. A large part of this flood of insights, such as the special theory of relativity, quantum theory and the electroweak gauge theory, was successfully summarised in one grand theory in the early 1970s [5].

2.1 The Standard Model

Today, all observable phenomena can be traced back to four fundamental interaction forces: gravitation, electromagnetism, strong and weak interaction. Latter three can be described by the Standard Model of particle physics (SM), whereby the fundamental issue of this theory was identified at the outset: the absence of inclusion of gravitational force. Furthermore, it does not explain the accelerating expansion of the universe, the ratio of matter and anti-matter in it and phenomena like neutrino oscillation. These are current problems with a need for solution. Nevertheless the SM is the most comprehensive description of physical phenomena to ever exist and and completely sufficient to form the theoretical basis for the problem discussed later in this work.

Within the framework of quantum field theory combining quantum mechanics and special relativity as the theoretical foundation, gauge bosons function as interaction mediators in between all known elementary particles. These are what we call matter and can be classified in two types of quarks and leptons with three generations of the same family, distinguishable by their increasing mass with generation. To each of these exists a corresponding antiparticle, which are what we call antimatter.

Interaction processes are representable in Feynman diagrams, which are pictorial representations of quantum field theory interactions. Based on simple rules, complex mathematical expressions can be derived and theoretical cross sections, being the measure of interaction probability, can be calculated.

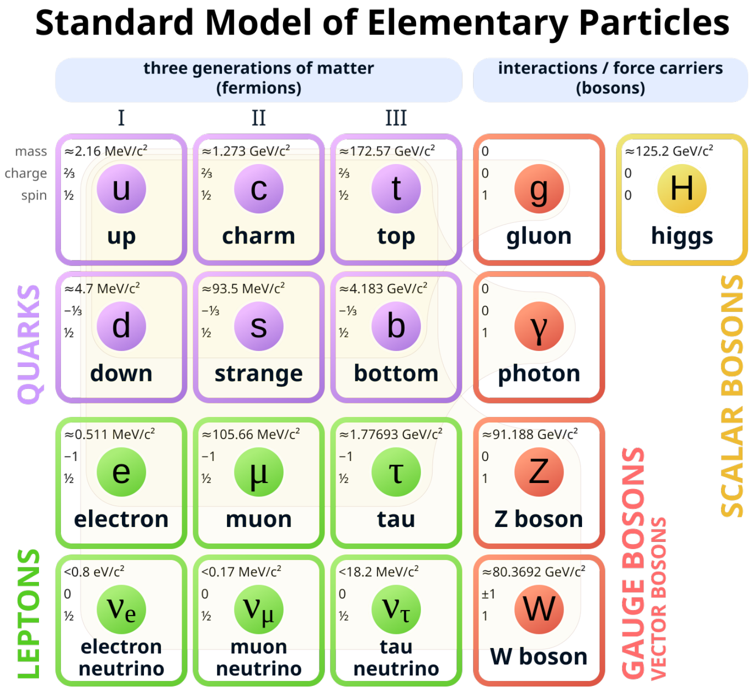

Figure 2.1: Elementary particles in the Standard Model[1].

Acting interaction forces correspond to the respective charge the particles carry. The strong interaction force describes the strong attraction of quarks in hadrons, e.g. protons, neutrons or mesons consisting of a quark antiquark pair. It is described by quantum chromodynamics, a non-abelian gauge theory based on the local SU(3) symmetry group. Its mediating gauge bosons, the gluons, do not carry an electric charge but a color charge, which comes in three types: red, blue and green with an anti color each. As quarks and gluon are the only particles carrying non-vanishing color charge, they only participate in strong interactions with each other.

A concept better known in everyday applications is the electromagnetic force, theoretically described by quantum electrodynamics (QED) with the symmetry group U(1). It is mediated by electrically uncharged photons, massless and spin-less just like the gluon [5, 6].

The unification of electromagnetic and weak interaction has led to some of the most important discoveries of the SM up until the 21st century and will be also be the relevant interaction in the processes important for this work. Therefore, we will examine it in more detail.

[1] Cush (`https://commons.wikimedia.org/wiki/File:Standard_Model_of_Elementary_Particles.svg`), „Standard Model of Elementary Particles“, `https://creativecommons.org/licenses/by/3.0/legalcode`

2.2 Electroweak interaction

The observation of β decay revealed the need to introduce a further interaction due to apparent energy and angular momentum conservation violation. A new particle without an electric charge and spin $1/2$ called neutrino was proposed. As the performing interaction force had a very short range compared to the QED, it was named the weak force, and should therefore be mediated by a heavy particle.

The solution was the introduction of a massive and charged mediation boson called $W^{\pm}$ (weak) boson. The theoretical unification with the QED, described with the SU(2)×U(1) gauge group demanded the existence of another, neutral, gauge boson. However, a lack of experimental indications, the so called "absence of neutral currents" prevented greater attention drawn to this theory in the physicist community. This was until 1973, when the experimental proof of inelastic neutrino-nucleon scattering succeeded. In the Standard Model, this process is described with the exchange of the Z (zero-charge) boson [5, 6].

These gauge bosons mediate interactions between both leptons and quarks, while a process involving a W boson changes the electric charge, the weak isospin and the flavour of participants. A process with a Z boson does not involve a charge, nor a flavour change. A Z decays with probabilities of around 70% in hadrons and 10% in pairs of oppositely charged leptons. The remaining 20% are not detected neutrinos. The W boson decays to roughly 68% into hadrons and to 32% into one charged lepton and a neutrino with corresponding generation [7], which is the phenomenon observable in β decay. As the neutrinos cross section is quite small, it is not easy to detect. While there are facilities dedicated to the measurement of neutrino properties, the detection in a particle accelerator is limited to missing momentum and angular momentum (spin) based on conservation laws. In 1983 both bosons were experimentally verified and their masses have been determined with increasing accuracy over time. The current values, resulting from the mean of different measurements are $m_{\mathrm{W}} = 80.3692 \pm 0.0133\,\mathrm{GeV}$ and $m_{\mathrm{Z}} = 91.1880 \pm 0.0020\,\mathrm{GeV}$ [7].

The introduction of the weak interaction led to the groundbreaking discovery of parity (mirror symmetry) violation, one of the least understood mechanisms in particle physics. A direct consequence of the spontaneously broken, non-abelian gauge theories is the existence of self interactions of electroweak gauge bosons. The self coupling of W, Z or γ can proceed trilinear via a triple Feynman diagram vertex (interaction point) or quartic, with four interacting particles linked to the same vertex. While the $\gamma\gamma \rightarrow WW/WZ$ interactions are predicted, the quartic $\gamma\gamma \rightarrow ZZ$ coupling is not present in the SM [3, 8]. A precise measurement of such processes can therefore confirm theoretical SM predictions or may be used to search for new physics.

A further important development was the question of the origin of the masses of the massive gauge bosons. As mass-bound gauge bosons can only be described with the aid of a scalar field in quantum field theory and the introduction of such led to the next surprise. It was presented as the Higgs field, being part of the theoretical structure called Higgs mechanism, named after its inventor. A new gauge boson with spin zero was predicted as the scalar Higgs-field related quant, the Higgs boson. The experimental verification of such a particle in 2012 completed the theoretical structure of the SM [6] and left the particle physics community with the task of digging in detail until the entirety of conflicts with this theory lay the foundation for a greater one.

2.3 Experimental verification - The ATLAS detector

We have come a long way since the first cyclotron was build in 1930 and as our theoretical understanding evolved, so has the ability to measure and reconstruct particle collisions with an ever increasing accuracy. The data used for this work is taken from the ATLAS detector. It is part of the CERN (European Organisation of Nuclear Research) infrastructure and detects effects of proton proton (pp) but also heavy ion collisions from the LHC (Large Hadron Collider). The charged particle beam is controlled and accelerated by 1232 supraconducting dipole magnets surrounding the beam pipe [9]. Due to relativistic principles, the maximum producible mass of decay products is limited by the invariant mass of the system, which corresponds to the total energy of the system in its center-of-mass frame. As the proton bunches are accelerated to almost light speed, high mass particles as the higgs, W/Z bosons and top quarks can be part of the recorded debris. The LHC is a ring collider with an circumference of 27 km and produces center-of-mass energies up to $\sqrt{s} = 13$ TeV with seven other detectors situated around, the largest being ALICE, CMS and LHCb [10].

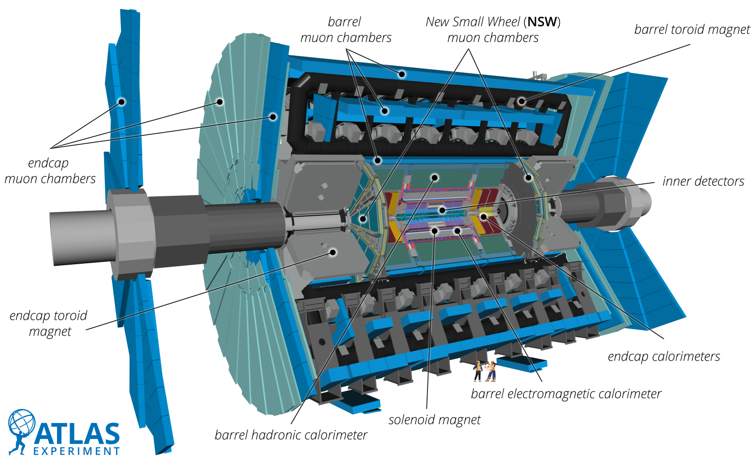

Figure 2.2: Schematic architecture of the ATLAS detector, image taken from Ref. [11].

The ATLAS detector is a almost hermetical cylindric structure along the longitudinal beam axis, subdivided into onion-like layers. The parameter that describes the number of particles collided over time and per area is the integrated luminosity L. It is given in the unit "per barn" with $1\,\mathrm{b}^{-1} = 10^{-28}\mathrm{m}^2$. Usually, all calculations in particle physics are done in natural units, meaning: the reduced Planck constant $\hbar$ and the speed of light c are set to the value 1 and SI units can be described in GeV.

In analysis, the interaction spot is set as the coordinate origin, with the longitudinal beam as z-axis while the x/y-plane is usually referred to as the transverse plane. Angular information is defined accordingly with the azimuthal angle φ and the polar angle θ. The latter is usually characterized by the pseudorapidity $\eta = -\ln(\tan\left(\frac{\theta}{2}\right))$

The inner detector is embedded in a magnetic field with the strength of $2\,\mathrm{T}$ produced by solenoid magnets and can therefore measure the momentum of electrically charged particles based on the curve of the trajectories induced by the Lorentz force. It covers a pseudorapidity range of $|\eta| < 2.5$ and is divided into three subdetectors: The high granularity silicon pixel, silicon microstrip and transition radiation tracking detectors.

The electromagnetic calorimeter runs with liquid argon as active detector material, while the hadronic calorimeter is scintillator-tile based. For both kinds of measurements, the pseudorapidity range is extended with liquid argon calorimeters at the endcap and forward regions to reach a $|\eta| = 4.9$. The muon spectrometer covers these calorimeters and is structured into three large superconducting air-core torodial magnets with eight coils each. Further, it includes precision tracking chambers and also fast detectors for triggering, leading to a maximum $|\eta| = 2.7$ [12, 13].

2.4 The $\gamma\gamma \rightarrow WW$ process

Particles experience the relativistic effect of Lorentz contraction when they are accelerated to high speeds. If the particle carries a charge and therefore an electric field, the latter gets compressed in the same way, leading to a high electromagnetic field strength in the plane perpendicular to the direction of movement.

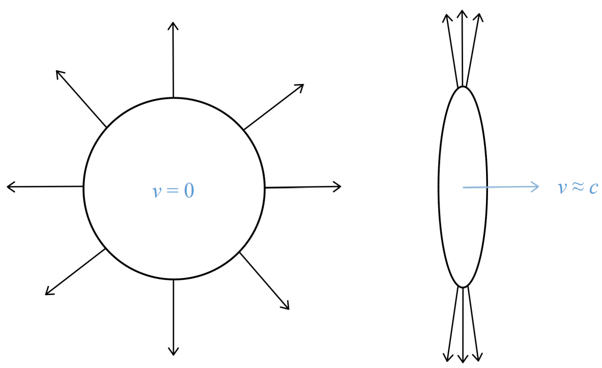

Figure 2.3: Simplified illustration of motionless and boosted charged particle and its electric field, sketch based on Ref. [14]

This electric field of two passing protons is an intense source of "quasi-real photons" which can transform into other intermediate particles or detectable leptons [15]. As intermediate photons do not have to satisfy the relativistic energy momentum relation $E = p \cdot c$ (they are "off shell"), "quasi-real" photons are intermediate photons with very low virtuality, meaning their energy and momentum are nearly those of real photons (they are almost "on shell"). Due to charge conservation, the resulting system must carry the electric charge zero. A process more recently predicted by the SM is the $\gamma\gamma \to W^+W^-$, which is depicted in the Feynman diagrams in Figure 2.4. Proceeding through trilinear (left) and quartic (right) W

Figure 2.4: Leading order Feynman diagrams for $\gamma\gamma \to WW$, image taken from Figure 1 in Ref. [4].

boson interactions, it only involves Feynman diagrams with self-couplings of the electroweak gauge bosons. Therefore, a study of properties, especially the verification of the theoretically determined cross section, directly tests the SU(2)×U(1) gauge structure, as deviations could indicate new physics beyond the SM.

An experimental verification of the existence of such process was successfully realized in 2016 on both, the ATLAS and CMS detector, independently [1, 2].

As the interacting photons transport high energies, the accelerated protons can potentially fragment. The nature of photon-photon interactions can therefore be differentiated into elastic, semi-dissociative and double-dissociative, referring to the protons remaining intact, one fragmenting and both fragmenting. When only the W boson final state particles (stable decay products) are reconstructed, the semi-dissociative interaction is still expected with the highest probability of 81%, while the least likely process is the double dissociative with only 3% [16]. While an elastic $\gamma\gamma \to WW$ interaction can be identified by the reconstruction of exactly two leptons with fitting properties, a dissociation leads to loads of byproducts emerging from hadronic decay of the proton(s). Together with a noneligible number of events overlapping per bunch crossing (collision of proton bunches), usually referred to as "pile up" events, this results in a difficult reconstruction and analysis of this process.

2.4.1 Event reconstruction and selection

The analysis this work follows, accessible in Ref. [4], is therefore optimized for the selection of elastic $\gamma\gamma$ interactions with candidate events being identified by the absence of any charged particle tracks besides the WW decay products. Those must be exactly one electron and one muon, as the cross section of a lepton pair production with a W intermediate is two orders of magnitude smaller than the cross section of the direct $\gamma\gamma \to \ell^+\ell^-$ process [15, 2]. However, as a pair of tauons (τ) can each decay into a neutrino and a W boson, this is the only $\gamma\gamma \to \ell\ell$ process not excluded by the criterion of an electron and muon containing final state. Due to a small number of such events, the influence is small as well.

In order to be considered in the analysis, an event first has to pass through track reconstruction criteria. Reconstructed with an iterative track-finding algorithm from a minimum of three hits (position measurements) in the inner detector (ID), tracks have to be compatible to an extrapolated trajectory.

Electrons are identified from energy clusters recorded in the electromagnetic calorimeter and then matched to the ID tracks [17]. Their p_T must exceed 20 GeV. The pseudorapidity must fulfill $|\eta| < 2.47$, excluding the calorimeter barrel-endcap transition, leading to a gap of detectable $|\eta|$ with $1.37 < |\eta| < 1.52$. Muons are directly identified from tracks in the muon spectrometer which are also matched to the ID tracks [18]. They have to fulfill $p_\mathrm{T} > 20\,\mathrm{GeV}$ and $|\eta| < 2.4$.

The tracks are then assigned to the same interaction spot, called vertex, which is reconstructed from the weighted average z position of their extrapolation to the beamline with equation (2.1). The number of tracks counted to the same event is within 1 mm of the vertex.

$$z_{\mathrm{vtx}}^{\ell\ell} = \frac{z_{\ell_1} \sin^2\theta_{\ell_1} + z_{\ell_2} \sin^2\theta_{\ell_2}}{\sin^2\theta_{\ell_1} + \sin^2\theta_{\ell_2}} \tag{2.1}$$

The lepton with the higher p_T of an event is the leading lepton with a minimum $p_\mathrm{T} = 27\,\mathrm{GeV}$. For the lepton with the second highest p_T, all requirements above apply. In this analysis as well as the following, other leptons will be considered for a better background estimation. Thereby, the track multiplicity n_trk will be the characteristic value for the number of tracks reconstructed additionally to the two leptons for one event.

2.4.2 Background estimation

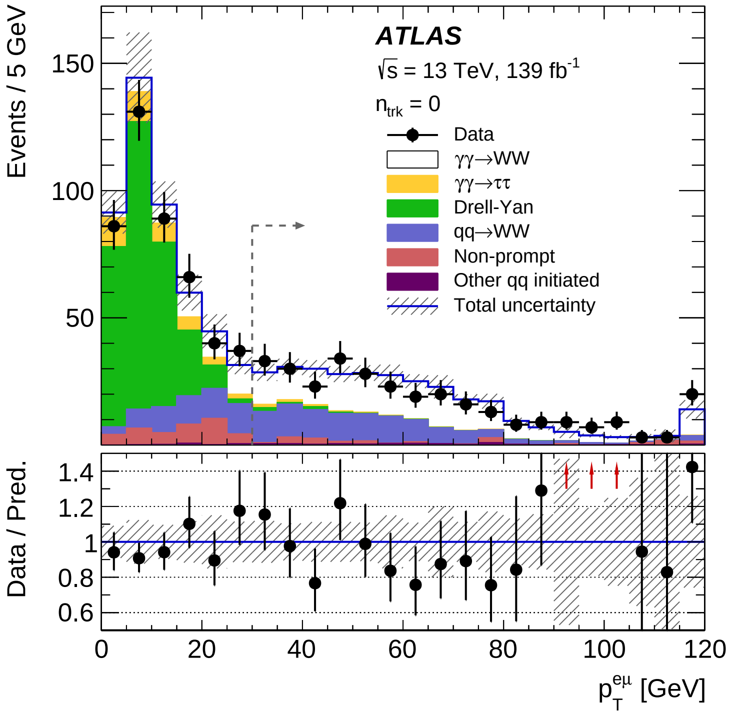

Figure 2.5: Distribution of the combined transverse momentum of both leptons $p_{\mathrm{T}}^{e\mu}$ with no other leptons detected, image taken from Figure 5 in Ref. [4]

A key concept for background estimation to this data set is the separation of phase space in signal and control region. The signal region is chosen, where the expected signal process is dominant or most likely to appear, while the control region is kinematically similar, but dominated by background events and has little or no signal contribution. The goal is the extrapolation of backgrounds in the signal region using simulation, scaling factors, or data-driven techniques with the data and estimations from the control regions. An important part of this estimation is the usage of Monte-Carlo generator based simulations, which can produce randomly sampled events based on an underlying theoretical model [19].

In the $\gamma\gamma \to WW$ analysis one signal and three control regions are defined based on the combined dilepton transverse momentum $p_{\mathrm{T}}^{e\mu}$ and n_{trk}. The signal region is chosen with $p_{\mathrm{T}}^{e\mu} > 30\,\mathrm{GeV}$ and $n_{\mathrm{trk}} = 0$, with an expected signal purity of 57% and 33% background contamination from $q\bar{q} \to WW$ production.

The expected backgrounds are mainly such $q\bar{q} \to WW$ events, which will be examined in more detail in the next section, and Drell-Yan events, characterized by the annihilation of a quark and antiquark pair, forming a virtual photon or Z boson: $q\bar{q} \to Z^*/\gamma^* \to \ell^+\ell^-$ (the Feynman diagram can be seen in Figure 2.6). Here, only the Drell-Yan processes with a $\tau^+\tau^-$ production will be considered, as the final state of equal leptons with opposite charge is excluded. Another noneligible part of the background are non-prompt leptons, which are not produced in the pp

hard scatter interaction but by secondary hadronic decay interactions and falsely assigned to the interaction vertex.

The first control region, $p_{\mathrm{T}}^{e\mu} < 30\,\mathrm{GeV}$ and $1 \leq n_{\mathrm{trk}} \leq 4$, is dominated by Drell–Yan ($Z/\gamma^* \to \tau\tau$) processes, which account for 75% of events, with additional contributions from $q\bar{q} \to WW$ and non-prompt leptons. The second control region, $p_{\mathrm{T}}^{e\mu} > 30\,\mathrm{GeV}$ and $1 \leq n_{\mathrm{trk}} \leq 4$, is enriched in $q\bar{q} \to WW$ events, contributing about 70% of events. The third control region, $p_{\mathrm{T}}^{e\mu} < 30\,\mathrm{GeV}$ and $n_{\mathrm{trk}} = 0$, provides additional control for background modeling and has a signal contamination of 10%.

A visualisation of this subdivision can be seen in Figure 2.5, where the grey line and arrow mark the begin of the signal region. With the estimation derived from the control regions, events in the signal regions can be scaled and the absolute background can be estimated. A detailed description can be found in Ref. [4] in chapter 6.

2.5 The $q\bar{q} \to WW$ background

As the modelling of the fragmentation of the proton relies on phenomenological concepts, the simulation of the charged particles produced from initial-state radiation or secondary partonic scattering, also called underlying events, is challenging. For a low number of detected charged particles, the underlying event distribution was found to be poorly modelled. For quark induced processes with a colourless final state (leptons or bosons), a comparability was assumed to estimate the $q\bar{q} \to WW$ background. This process, as well as the production of WZ and ZZ (however, negligible in this analysis) will be referred to as diboson production.

2.5.1 Correction derived from Drell-Yan

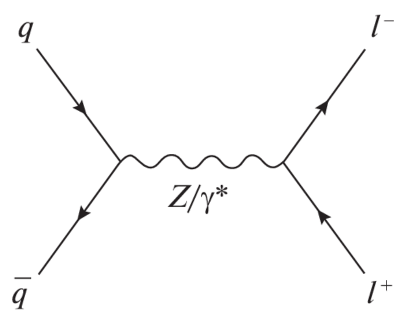

Figure 2.6: Feynman diagrams for the Drell-Yan process mediated by $Z/\gamma*$ to dilepton final state, image taken from Figure 1 in Ref. [20]

The estimation of this specific background process was derived from using data measurement of Drell-Yan production, specifically via a Z boson. While Monte-Carlo samples of different simulations vary with large differences for the track multiplicity spectrum of charged particles, the behaviour of the diboson and Drell-Yan spectra can be considered similar within 10-20% at a constant diboson p_T. Events are selected using the similar criteria described in Section 2.4.1 with an additional requirement for the dilepton mass around the Z mass value with $70\,\text{GeV} < m_{\ell\ell} < 105\,\text{GeV}$. An important difference in selection is the final state consists here of same flavour leptons. The background is dominated by $\gamma\gamma \to \ell\ell$ events, which are subtracted using a fit in a $p_T^{\ell\ell}$ control region, as the kinematic properties are distinguishable from Drell-Yan. Influence from $\gamma\gamma \to WW$ is neglected, as it is expected to be less than 1% in that region. Pile-up track influences are minimized by using data driven techniques based on reweighting, corrections of the beam spot width and ancillary measurements, counting tracks near a random z position well separated from the interaction vertex with at least 10 mm.

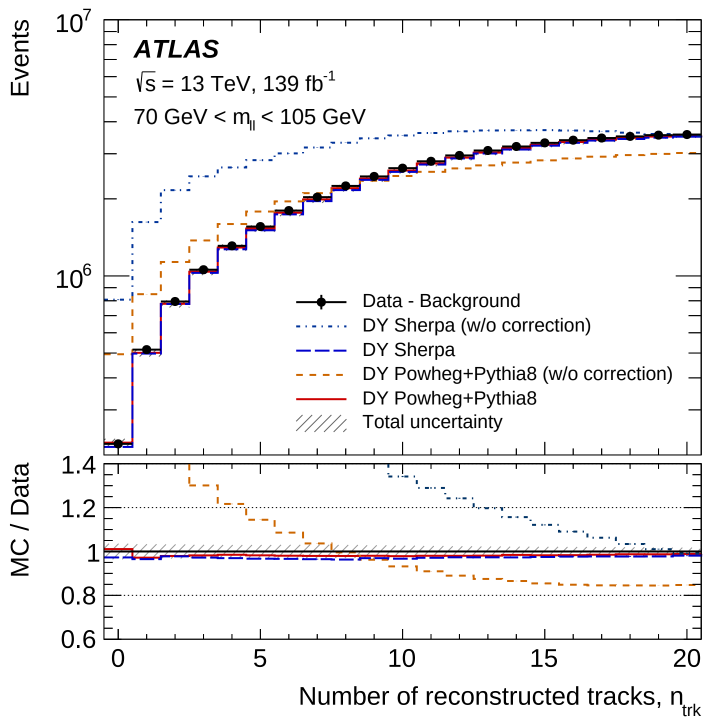

Figure 2.7: Comparison of the match of data and Monte-Carlo models Sherpa and Powheg+Pythia8 before and after appliance of per-event weight correction for the track multiplicity n_{trk}, image taken from Figure 3 in Ref. [4].

After the subtraction of backgrounds, D'Agostini unfolding [21, 22] is applied on the distribution of n_{trk} as a function of $p_T^{\ell\ell}$. With the ratio of unfolded data to unfolded simulation values as a function of the charged-particle multiplicity and dilepton transverse momentum emerging from the Z decay, the charged particle multiplicity of modelled Drell Yan events is adjusted with per-events weights. The results can be seen in Figure 2.7, where Sherpa and Powheg+Pythia8 predictions before and after corrections and the data are plotted for $0 \leq n_{\text{trk}} \leq 20$. The best fitting model was Powheg+Herwig7, which is not shown in this plot, exceeded the data with about 30%. All simulations now align well within uncertainties. This correction, depending on n_{trk} and the p_T of reconstructed decay products is then applied to the diboson $pp \to WW/WZ/ZZ$ processes as well, leading to an approximation of this background distribution observable in Figure 2.8. Here, the track multiplicity is shown for up to five tracks. The uncertainties of the track reconstruction result from the alignment of the inner detector and the reconstruction efficiency. The probability of falsely reconstructed tracks with a consideration of detector background noise is also included. Simulation uncertainties result mainly from pile-up tracks and the distributions before the corrections, assessed by the comparison of POWHEG+PYTHIA8 and SHERPA. They are and can be expected to be relatively small.

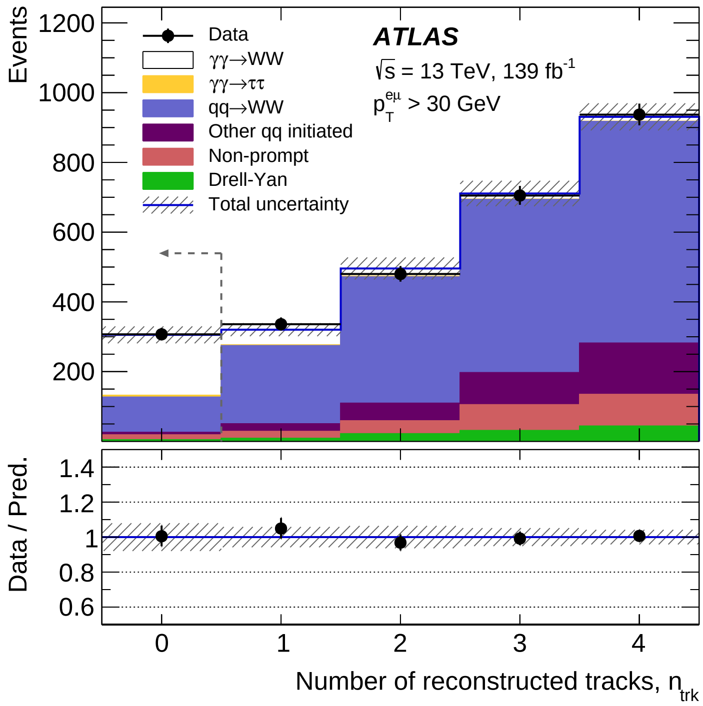

Figure 2.8: Distribution of track multiplicity after corrections applied, image taken from Ref. [4]

This estimation is only justified by a similarity in Monte-Carlo samples, while the differences of Drell-Yan and diboson prediction are up to 20%. Therefore, a validation of the conducted reweighting is necessary. A process with physical properties comparable to the $q\bar{q} \to WW$ production is $q\bar{q} \to WZ$.

2.5.2 Qualitative comparability to $pp \to WZ$

As the transfer of the corrective function from Drell-Yan simulation adjustment was rather born out of necessity, another control region to validate this estimation is needed. A process suitable for comparison is the $q\bar{q} \to WZ$ production. If the reweighted simulated events correctly depict the selected data for this process, the same can be assumed for $q\bar{q} \to WW$. The similarity of the diboson production can be derived from the comparison of Feynman diagrams in Figure 2.9.

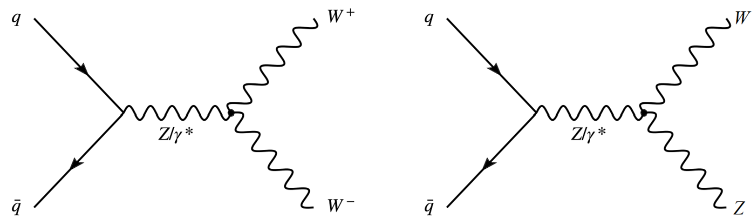

Figure 2.9: Leading order Feynman diagrams for the $q\bar{q}$ annihilation to a WW and WZ final state, image taken from Figure 1 in Ref. [23]

While the cross section is much smaller than WW production [24], its final state is not as challenging in reconstruction. This is due to the production of three charged leptons and one undetected neutrino, while the WW final state includes two neutrinos and can therefore only be differentiated by the missing energy of both neutrinos. Despite the large difference in detected events, a qualitative comparability regarding the n_{trk} spectra can be expected. Therefore, the study of the track multiplicity of the $pp \to WZ$ process is suitable as a control sample for the $pp \to WW$ background from the $\gamma\gamma \to WW$ analysis.

3 Selection of a $pp \to WZ$ control sample

In this chapter, the development of the $pp \to WZ$ selection will be presented. The goal will be the provision of a reliable WZ control region to validate the reweighting of the charged particle multiplicity done in the $\gamma\gamma \to WW$ analysis for $pp \to WW$ background events. For this purpose, the preselected data will be analyzed and optimized by the evaluation of mass and momentum variables and the kinematic properties of WZ events reconstructed. Lastly, cuts (the setting of boundaries on these variables) on the basis of known values will be applied.

To understand the following procedure, we have to take a look at the situation we are starting with. To provide a reliable control region, it is necessary to filter out all kinds of events other than $pp \to WZ$. In Figure 3.1, the track multiplicity of this process is shown. Which means in this case, the number of tracks reconstructed additionally to those of the W and Z boson decay products.

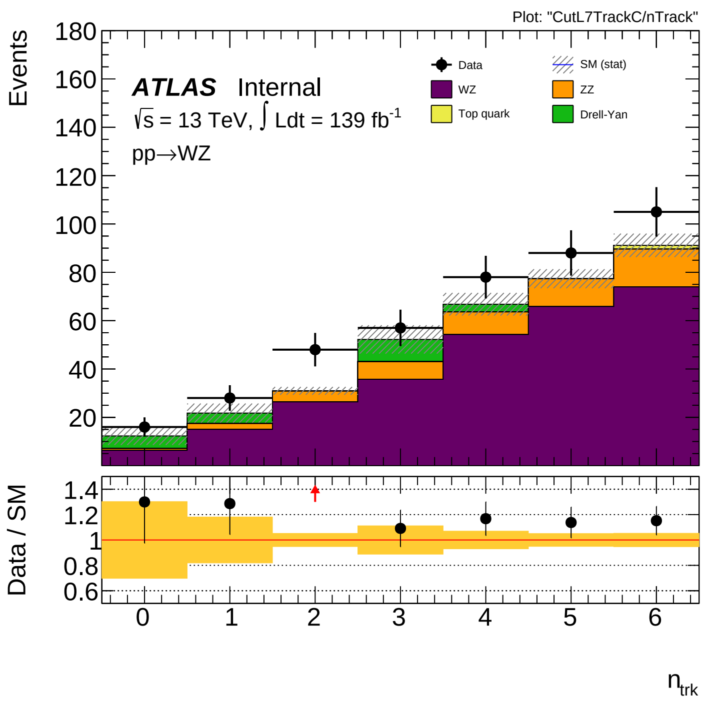

Figure 3.1: Track multiplicity with only pre-cuts applied.

The plots presented in this analysis depict expected top quark pair production, Drell-Yan processes, $qq \to WZ$ and $qq \to ZZ$ production. The yellow coloured area in the data to simulation ratio bar below shows the simulation uncertainties, which are represented by the hatched area in the original plot. To ensure a good statistical significance, up to seven additional tracks will be allowed in the following analysis.Just looking at the histogram, one quickly comes to realize that the data and simulation do not match very well and there seem to be events the simulation is not able to predict. This is mainly due to the difficult detector simulation and the resulting lack of exclusion of misidentified leptons, which are usually hadronic jets that imitate a lepton signal. Moreover, the fragmentation of the protons and the resulting scattering of particles with a small momentum exchange and scattering angle can not be described by perturbative quantum field theory. The simulation of such relies on phenomenological models, which can not be performed with the same precision.

The events selected contain Drell-Yan events, since its final state is a pair of oppositely charged leptons and can therefore be incorrectly assigned as the Z decay without a closer kinematic selection. A small percentage of $pp \to WW$ events is also expected, however, being negligible with a cross section about four orders of magnitude smaller then Drell-Yan events [25, 23]. Top quarks can decay into a bottom quark and a W boson, which can be falsely assigned to the $pp \to WZ$ process. The goal of the following chapter will be the exclusion of these background events, to provide a better consistency of simulation and data, and an enhanced purity of selected $qq \to WZ$ events accordingly. The ZZ production is mostly irreducible background. With four charged leptons in final state, it can contribute to $n_{\mathrm{trk}} > 0$ and with a lepton falling outside of the detectors acceptance, to $n_{\mathrm{trk}} = 0$ as well [26].

3.1 Preselection

Simulated events were generated with the Monte Carlo generator Powheg+Pythia8 and need to pass through a detailed model of the ATLAS detector based on Geant4 [27].

The data used for this analysis are pp collisions with 139 fb^{-1} that have been recorded between 2015 and 2018 at the ATLAS detector with an average of 33.7 collisions per bunch crossing. To be considered for this analysis, it must fulfill certain basic criteria very similar to the analysis described in Ref. 2.4.1 and [4]. The candidate events are selected by requiring three charged leptons, which can be electrons or muons. The leading leptons need to be detected with a minimum transverse momentum p_{T} of 27 GeV, subleading are required to have at least 15 GeV. Other leptons need to meet the requirement of $p_{\mathrm{T}} > 10\,\mathrm{GeV}$. The pseudorapidity electrons can be detected with is limited by the detector acceptance and therefore the data is precut to $|\eta| < 1.37$ or $1.52 < |\eta| < 2.47$. Due to the structure of the muon spectrometer, muons are precut to a range of $|\eta| < 2.4$.

Both muons and electrons need to pass 'loose' identification selection criteria, referring to the number of hits in the inner detector and the electromagnetic calorimeter or the muon chamber

[18]. A further 'medium' selection of the electrons is based on the discriminant value of a likelihood identification [17] which is constructed using the shape of the electromagnetic showers, the track properties from the inner detector and how well these fit together. Most importantly, all events considered must include exactly four charged leptons, of which only three can be detected as one neutrino is produced. Therefore, the W candidate can be reconstructed best, when the missing neutrino detection is considered, which will be discussed in the next section. The Z boson decays into two oppositely charged leptons of the same flavour.On this basis, further selection criteria beyond the general preselection for all leptons considered are applied. For the Z candidate, pairs of oppositely charged leptons of same flavour are selected. For this, the lepton pair with a combined four momentum sum (invariant mass) closest to the Z mass is selected. The single W lepton is chosen depending on being an electron or muon. To be assigned to the W boson, electrons now need to pass a tight likelihood and isolation identification criterion. Muons must pass a tight isolation criterion.

3.1.1 Reconstruction of kinematic properties of the W boson

For accurate reconstruction of the W-boson mass and kinematics, the estimation of the missing neutrino momentum is essential. This is calculated using conservation of momentum in the transverse plane of the event, meaning: the transverse momentum $\vec{p}_{\mathrm{T}}$ of all detected particles is vectorially summed. As the total momentum in the transverse plane must be preserved, this vector sum should vanish but since the neutrino is not detected, its transverse momentum results from this vectorial sum over all detected charged particles. Therefore, the total missing tranverse momentum $\vec{p}_{\mathrm{T}}^{\mathrm{miss}}$ per event results from equation (3.1).

$$p_{\mathrm{T}}^{\mathrm{miss}} = |\vec{p}_{\mathrm{T,leptons}}^{\mathrm{miss}} + \vec{p}_{\mathrm{T,hadrons}}^{\mathrm{miss}}| \tag{3.1}$$

The contributions of reconstructed leptons and remaining (mostly hadronic) tracks of the event are shown in Figure 3.2. The influence of hadronic tracks is limited to low missing transverse momenta, whereby most of their momentum vectors cancel to zero. The neutrino momentum $p_{\mathrm{T}}^{\mathrm{miss}}$ results mostly from the lepton selection. For the combined $p_{\mathrm{T}}^{\mathrm{miss}}$, the highest data values accumulate from 7.5 GeV to 30 GeV and decrease with increasing momentum, while the expected WZ event peak is from 30 GeV to 37.5 GeV. The data below 30 GeV exceeds the simulation predicted values. The histogram for the neutrinos momentum $p_{\mathrm{T}}^{\mathrm{miss}}$ is depicted in Figure 3.3.

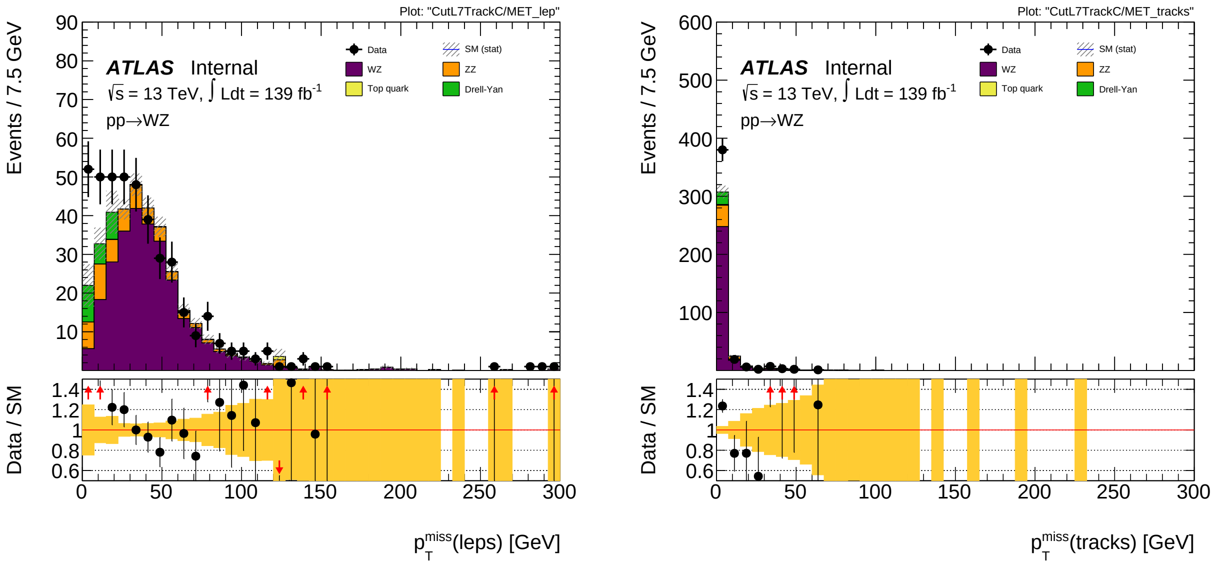

Figure 3.2: Contribution of missing transverse momentum of detected leptons (left) and hadronic tracks (right).

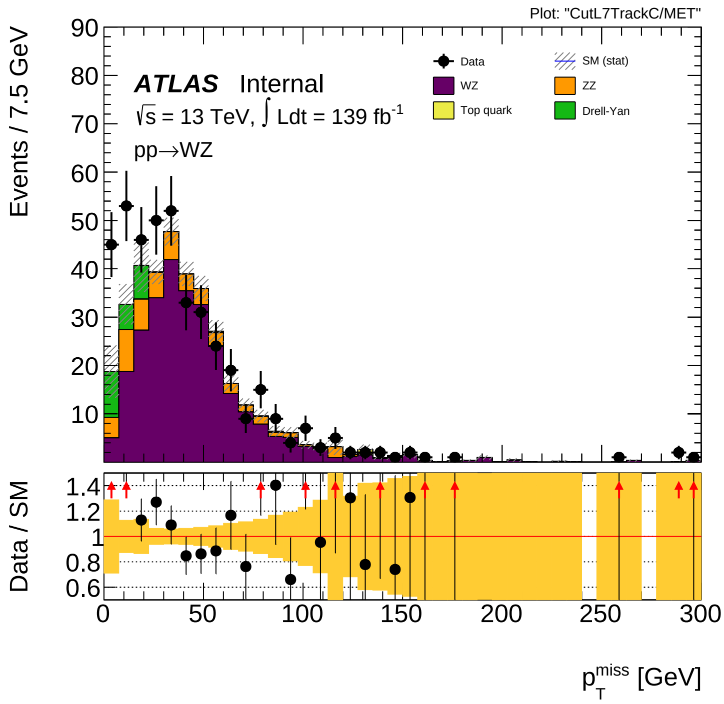

Figure 3.3: Total missing transverse momentum of neutrino.

Hence, an consideration of the W mass is practical as its value is well determined and will therefore be used as a guiding and cutting variable. However, due to a missing information of the longitudinal component of the neutrino momentum, only the transverse mass can be estimated using equation (3.2), resulting from the relativistic energy-mass relation and momentum conservation in the transverse plane. Here is $\Delta\phi$ the azimuthal angle between the vectors of the charged lepton and the neutrino.

$$m_{\mathrm{T},W} = \sqrt{2 \cdot p_{\mathrm{T}}^{\ell} \cdot p_{\mathrm{T}}^{\nu} \cdot (1 - \cos \Delta\phi)} \tag{3.2}$$

The resulting histogram in Figure 3.4 shows one event peak expected to be mostly Drell-Yan events from about 10 GeV to 20 GeV. The most events are recorded for $72 < m_{\mathrm{T},W} < 84$ GeV with a steeper decline towards higher values then to lower $m_{\mathrm{T},W}$. Following from the definition of the transverse mass, the values range with an upper limit of the full W mass, as information from the longitudinal direction is lost due to pure consideration of the transverse plane. The value of the transverse mass of the W boson therefore matches the total invariant mass, if the W system is produced at rest [28] with a scattering angle between neutrino and charged lepton $\Delta\phi = 90°$. Events above $m_{\mathrm{T},W} = m_W$ result from the width of reconstructed variables and the resolution of the detector.

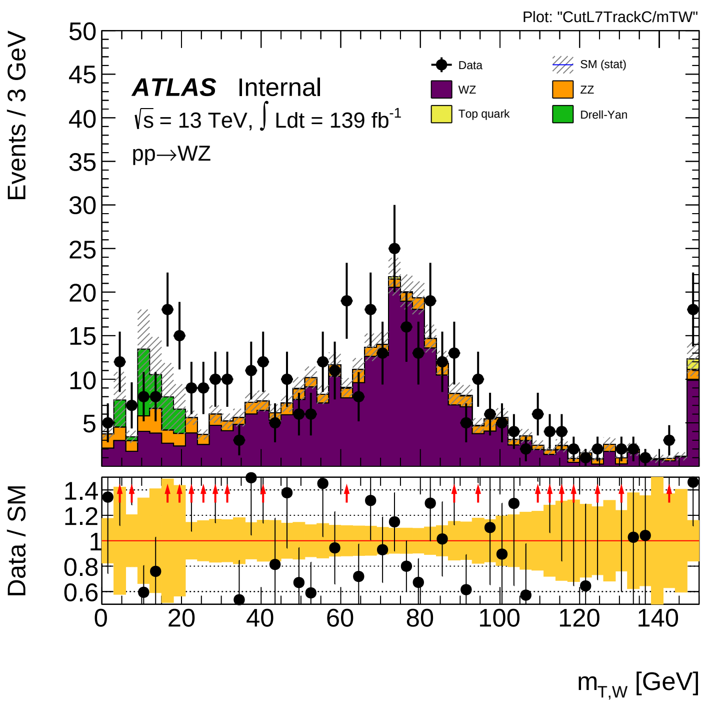

Figure 3.4: Transverse mass of the W-boson.

3.1.2 Mass of the Z boson

Since the Z boson decays into two oppositely charged leptons with fully reconstructed four momentum, the calculation of invariant mass is possible and can be done with a higher resolution than the transverse W mass. It is determined by summing the four momenta in form of equation (3.3).

$$m_Z = \sqrt{(E_{\ell^+} + E_{\ell^-})^2 - (\vec{p}_{\ell^+} + \vec{p}_{\ell^-})^2} \tag{3.3}$$

The full knowledge of decay products related to the Z leads to a resonance-like peak in its mass distribution. Another salient feature is the appearance of an event peak resulting from the preselected cut on p_{T} at 25 GeV in a threshold at 50 GeV and is therefore low p_{T} background activity.

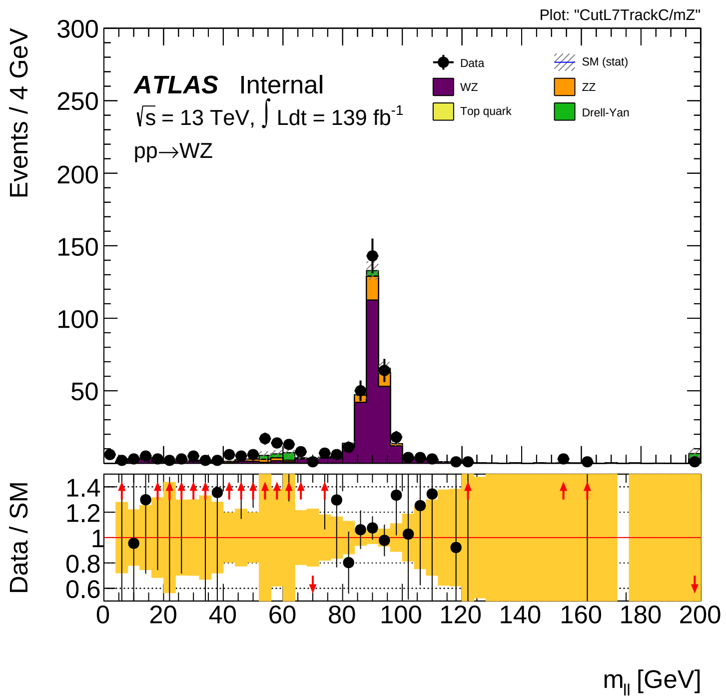

Figure 3.5: Invariant mass of the Z-boson.

3.2 Selection

The goal of this section will be the largest possible exclusion of background events disrupting the variables discussed without loosing too many WZ events and therefore statistical significance. For this, cuts will be applied to exclude sensible events as non-simulatable processes, Drell-Yan and misidentified leptons.

3.2.1 Neutrino momentum and transverse mass of the W boson

Due to distribution of events in the W transverse mass and neutrino momentum histogram and the well determination of the W mass value, a cut for on the W transverse mass variable was applied. In consideration of the peak at around 10 GeV, which is mainly expected to be Drell-Yan events, a cut of 40 GeV around 80.364 GeV was chosen, which can be seen in Figure 3.6.

As the amount of selected events is not very large, the cut was not chosen slimmer, since the statistical significance increases with the number of events. Further, it was not chosen with a lower higher limit, since the events above m_W are still expected to be WZ events. This leads to a complete exclusion of simulated Drell-Yan events and events derived from other processes besides $pp \to WZ$ and $pp \to ZZ$ in neutrino momentum p_T^{miss}, which can be seen in Figure 3.7. The data and simulation now align well for $p_T^{miss} < 30$ GeV, resulting in a significant maximum at 30 GeV to 37.5 GeV.

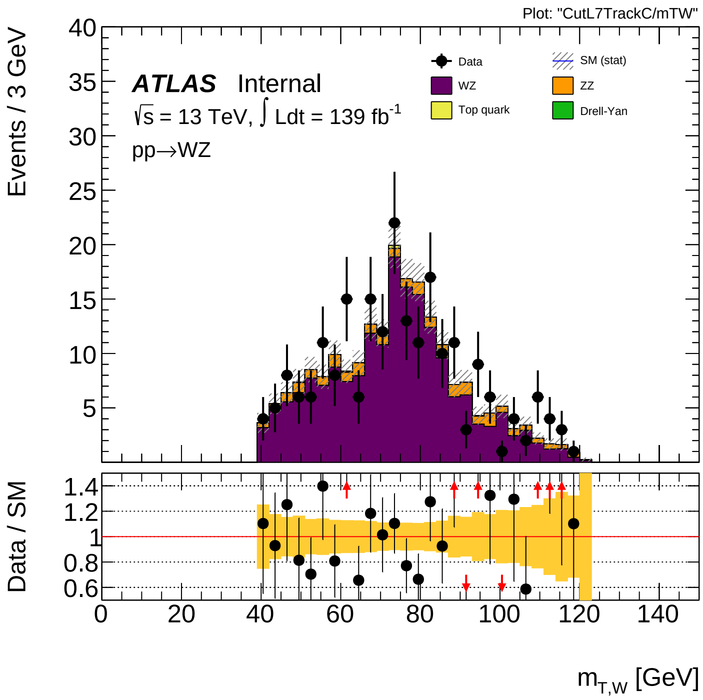

Figure 3.6: Transverse mass of the W-boson with cuts applied.

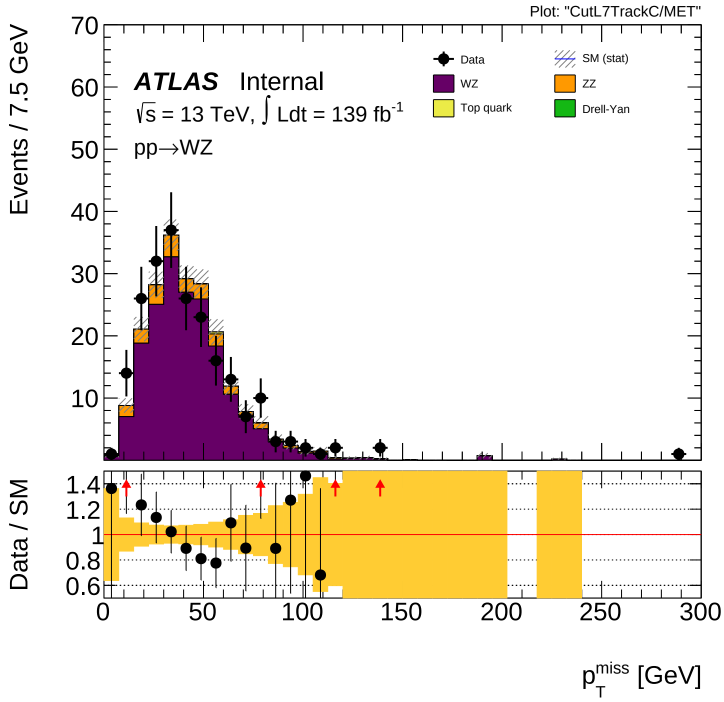

Figure 3.7: Total missing transverse momentum of neutrino after W_m cut applied

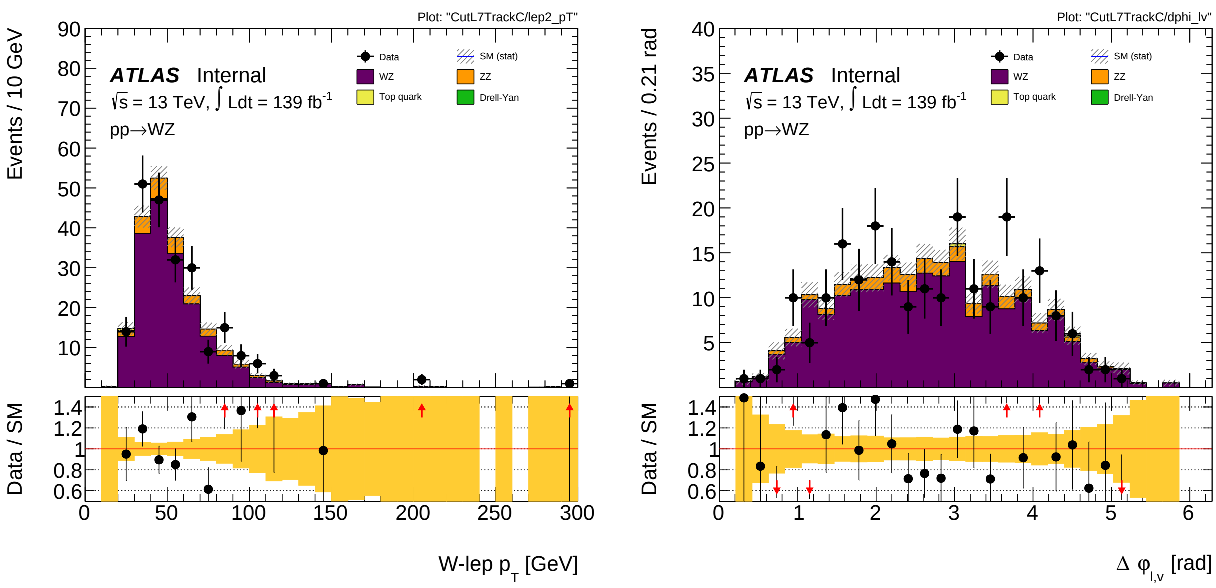

Figure 3.8: Transverse momentum of the lepton assigned to the W boson (left) and angle between lepton and neutrino emerging from the W boson (right).

From this, we can conclude that the cut on the W mass has led to a large exclusion of events that do not produce neutrinos or a W boson without a heavy loss of events overall. However, with all cuts applied simultaneously, the peak now carries less events, because of the exclusion of events in the Z mass cut, which will be discussed in the next section. Further, the distribution of the angle between lepton and neutrino $\Delta\phi$ meets the expectation with an even distribution around π, which can be taken from the left plot in Figure 3.8. The transverse momentum of the lepton assigned to the W boson is shown in the right plot of Figure 3.8 with a maximum of events at 30 GeV to 50 GeV.

When the W system is produced at rest, the neutrino and charged lepton transverse momentum should approximately be half the W mass [28]. Resulting from the distributions of these variables, this seems to be the case for most selected events, with small losses to the longitudinal direction and resolution limitations.

3.2.2 Mass of the Z boson

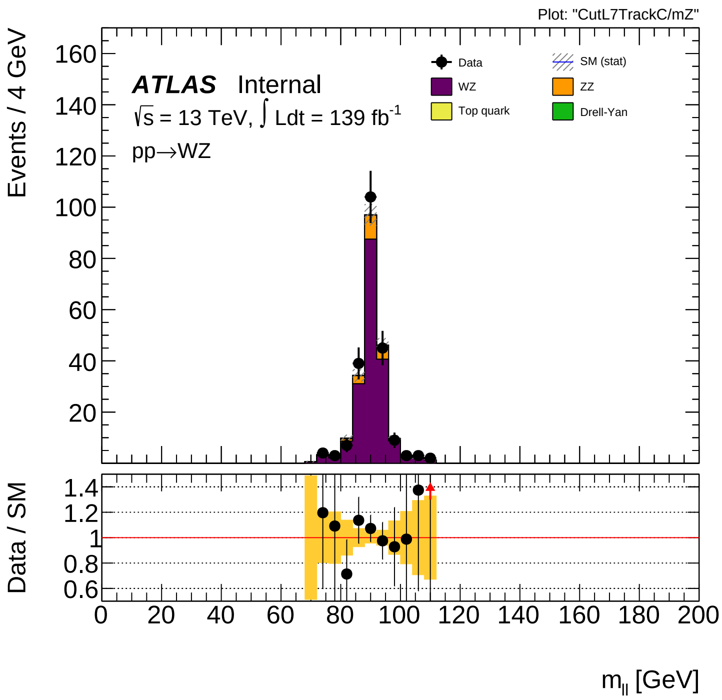

Figure 3.9: Invariant mass of the Z boson with cuts applied.

The distribution of the invariant Z mass being concentrated at the theoretical value with little events at other energies allow the cut applied to be chosen tighter than for the W boson. It was chosen to be 20 GeV around the latest value of $Z_m = 91.188$ GeV [7], which can be seen in Figure 3.9.

As the cut was performed simultaneously to the W mass cut, the resulting peak in the histogram in 3.9 carries less events as well and the predicted Drell-Yan events in the peak are excluded. This is due to the exclusion of events in the W mass cut that produced leptons assigned to the Z decomposition.

3.3 Results

After all mass cuts applied, one can take a look at the final track multiplicity histogram, however a few preliminary considerations are useful. This section will provide a statistical testing method and a detailed analysis of the outcome.

3.3.1 Performance of χ^2 tests

To evaluate the fidelity of the simulation and agreement with the filtered data, χ^2 tests are performed. For this, the absolute χ^2 value was calculated according to equation (3.4). The standard deviation for each bin (histogram bar) results from the uncertainties of data and simulation by equation (3.5).

$$\chi^2 = \sum_{i=1}^{N_{\text{bins}}} \frac{(O_i - E_i)^2}{\sigma_i^2} \tag{3.4}$$

$$\sigma_i = \sqrt{(\sigma_{\text{data}}^{\text{err}})^2 + (\sigma_{\text{simulation}}^{\text{err}})^2} \tag{3.5}$$

O_i : Observed data value
E_i : Expected/Simulation value
N_{bins} : Number of bins (histogram bars)
σ^{err} : Uncertainty of data/simulation value.

Therefore, a bad match of data and simulation can be identified by the comparison number of degrees of freedom (number of bins) and the χ^2 value and its magnitude. Therefore, the χ^2 values will be given as the ratio of both. A bad match would be identified with a $\chi^2 \gg N_{\text{bins}}$ and $\chi^2/N_{\text{bins}} \gg 1$. However, this method does not provide precise information of the quality of the match [19].

3.3.2 Final track multiplicity

The track multiplicity after the final WZ selection depicted in Figure 3.10 represents a great improvement compared to the preselection. The selection led to a complete exclusion of expected Drell-Yan and top quark events with now only WZ and few ZZ events in track multiplicities greater than zero expected.

Simulation and data align much better with an enhancement of the χ^2 value from $\chi^2_{\text{pre}}/7 = 11.18/7 \approx 1.60$ to $\chi^2_{\text{sel}}/7 = 2.01/7 \approx 0.3$. All bins align well within uncertainties apart from $n_{\text{Track}} = 0$, where the data still exceeds the simulation value.

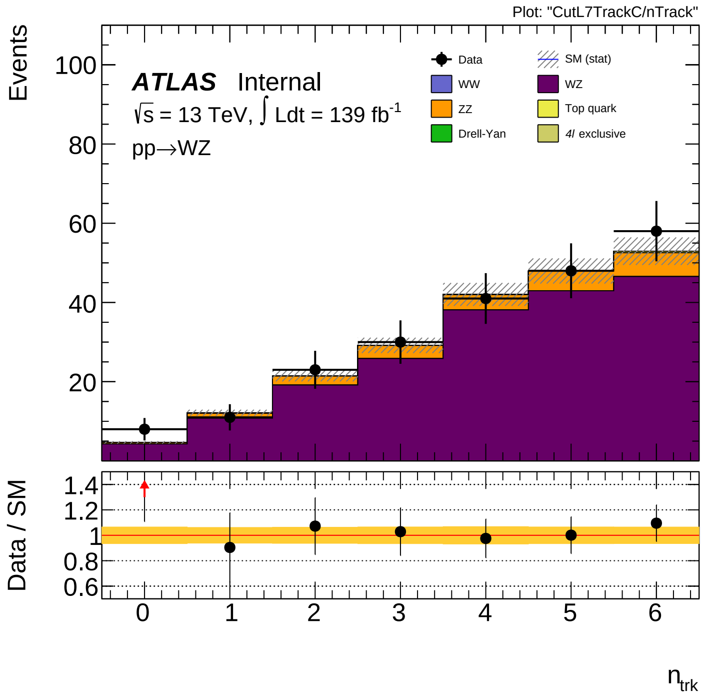

Figure 3.10: Number of reconstructed additional tracks after selection.

3.3.3 Charge distinction of the W boson

To study the event excess in the $n_{\text{Track}} = 0$ bin in more detail, the track multiplicity distribution presented in the last section is separated by charge of the W assigned lepton. This can be seen in Figure 3.11. As the $qq \to WZ$ process is initiated by the scattering of positively charged protons (consisting of two up and one down quark, increasing the probability for positively charged particles forming) the share of $qq \to W^+Z$ decomposition is larger than its negative counterpart.

The expectation of significantly more events associated with W^+ boson was met and the expected values of data and simulation of $n_{\text{Tracks}} = 0$ fit very well within a tolerance range of 10% and within uncertainties with $\chi^2_{n_{\text{trk}}=0} = 0.02$. The related χ^2 value for all seven bins fits the visually recognizable similarity with $\chi^2/7 = {}^{1.45}/_{7} \approx 0.21$. For negatively charged W, the simulation of $n_{\text{trk}} = 0$ does not align well with the data, with a $\chi^2_{n_{\text{trk}}=0} = 1.92$. The overall match of expectation and data is sufficient with an overall value of $\chi^2/7 = {}^{4.76}/_{7} \approx 0.68$.

Unfortunately, the charge differentiation does not provide an answer to the high event yield in the first bin. For the negative W boson, the data exceeds the simulation by a range of 150% to 350%, considering the statistical uncertainties of the data. This requires further investigations with a more detailed causal research concerning the $n_{\text{Tracks}} = 0$ bin.

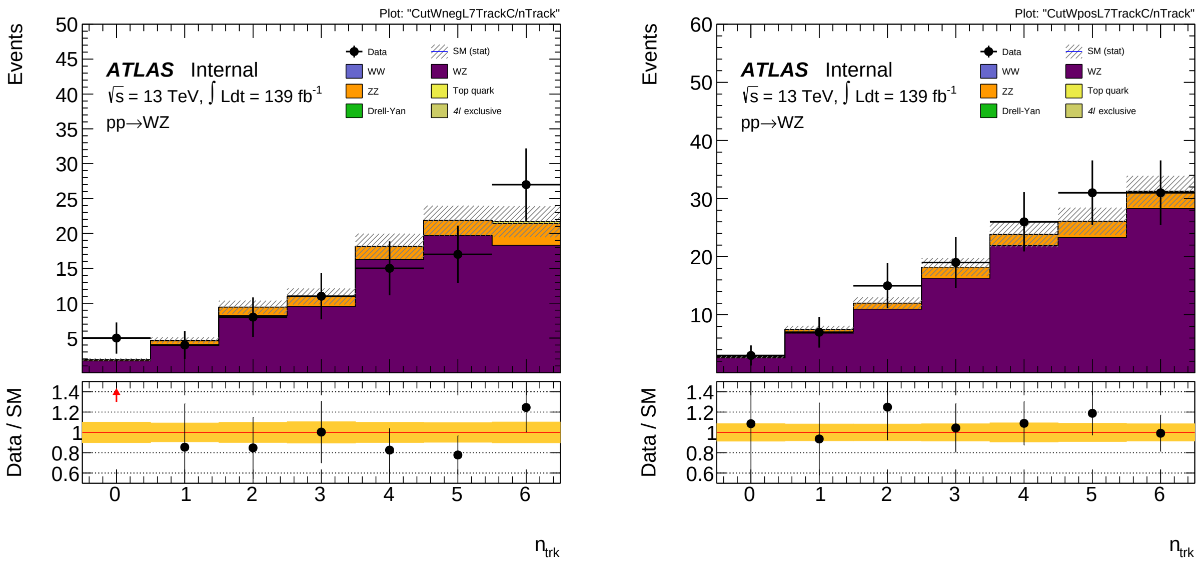

Figure 3.11: Number of reconstructed additional tracks with leptons emerging from W^- (left) or W^+ boson (right).

4 Summary and Outlook

In this work, a selection of $q\bar{q} \rightarrow WZ$ events was performed to provide a reliable control sample to validate the $q\bar{q} \rightarrow WW$ background estimation derived from Drell Yan events, done in the 2021 $\gamma\gamma \rightarrow WW$ ATLAS Collaboration analysis [4].

Events from data collected at the ATLAS detector were selected with preselection criteria based on requirements for the transverse momentum, pseudorapidity and most importantly, the number of detected leptons. With the WZ final state containing three charged leptons and a neutrino, events were selected with a minimum of three reconstructed leptons to the same vertex with an allowed track multiplicity up to $n_{\mathrm{trk}} = 7$.
Based on the preselected events, a selection on kinematic properties characteristic to WZ events was performed. This was done with the calculation of the missing momentum of the neutrino in the transverse plane and the p_{T} of the detected lepton assigned to the W boson to reconstruct the transverse W mass $m_{\mathrm{T},W}$. Further, the invariant Z mass m_Z was reconstructed with the four momenta of the Z assigned leptons.

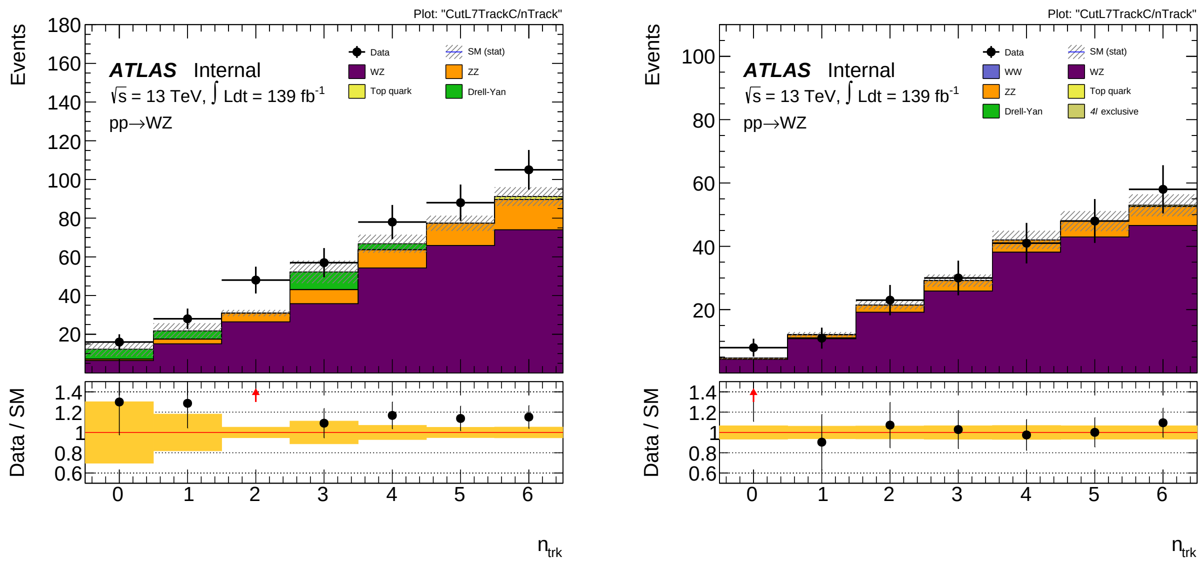

Figure 4.1: Number of reconstructed additional tracks before (left) and after (right) selection.

This led to a large exclusion of expected background and a high purity of selected WZ events. The reweighted Powheg+Herwig7 simulation expectancy was found to be in very good agreement with the data for $n_{\mathrm{trk}} > 0$ and can therefore be taken as a verification of the $q\bar{q} \to WW$ event reweighting. For $n_{\mathrm{trk}} = 0$, the data still exceeds the theory prediction and in a charge distinction of the W boson, large deviations were found for negative W assigned leptons. These differences of unexplained origin reveal the need for further studies of the $n_{\mathrm{trk}} = 0$ region of WZ events with a more detailed examination of a charge segregation of the W boson.

Overall, this study can be used in future analyses and the Drell-Yan derived $q\bar{q} \to WW$ background estimation was validated under the condition of further examinations regarding the $n_{\mathrm{trk}} = 0$ event bin. The track multiplicities after the preselection (left) and the final selection (right) can be taken from Figure 4.1.

Selbstständigkeitserklärung

Hiermit erkläre ich, Amalia Beer, dass ich diese Arbeit im Rahmen der Betreuung am Institut für Kern- und Teilchenphysik ohne unzulässige Hilfe Dritter verfasst und alle Quellen als solche gekennzeichnet habe. Ich reiche sie erstmals als Prüfungsleistung ein. Mir ist bekannt, dass ein Betrugsversuch mit der Note "nicht ausreichend" (5,0) geahndet wird und im Wiederholungsfall zum Ausschluss von der Erbringung weiterer Prüfungsleistungen führen kann.

Amalia Beer
Dresden, 9. Dezember 2024

5 Bibliography

[1] ATLAS Collaboration: Measurement of exclusive $\gamma\gamma \to W^+W^-$ production and search for exclusive Higgs boson production in pp collisions at $\sqrt{s} = 8\,\text{TeV}$ using the ATLAS detector. (2016)

[2] CMS Collaboration: Evidence for exclusive $\gamma\gamma \to W^+W^-$ production and constraints on anomalous quartic gauge couplings in pp collisions at $\sqrt{s} = 7$ and $8\,\text{TeV}$. (2016)

[3] Chapon, E. ; Kepka, O. ; Royon, C.: Anomalous quartic $WW\gamma\gamma$, $ZZ\gamma\gamma$, and trilinear $WW\gamma$ couplings in two-photon processes at high luminosity at the LHC. In: *Phys.Rev.D81:074003,2010* 81 (2009), April, Nr. 7, S. 074003. `http://dx.doi.org/10.1103/physrevd.81.074003`. – DOI 10.1103/physrevd.81.074003. – ISSN 1550–2368

[4] ATLAS Collaboration: Observation of photon-induced W^+W^- production in pp collisions at $\sqrt{s} = 13\,\text{TeV}$ using the ATLAS detector. (2021). `http://dx.doi.org/10.1016/j.physletb.2021.136190`. – DOI 10.1016/j.physletb.2021.136190

[5] Ecker, Gerhard: *Teilchen, Felder, Quanten: von der Quantenmechanik zum Standardmodell der Teilchenphysik*. Berlin: Springer Spektrum, 2017

[6] Thomson, Mark: *Modern Particle Physics*. Cambridge University Press, 2013

[7] Navas, S. and others: Review of particle physics. Version: 2024. `http://dx.doi.org/10.1103/PhysRevD.110.030001`. 2024. – DOI 10.1103/PhysRevD.110.030001, S. 030001

[8] Aihara, H. ; Barklow, T. ; Baur, U. ; Busenitz, J. ; Errede, S. ; Fuess, T. A. ; Han, T. ; London, D. ; Ohnemus, J. ; Szalapski, R. ; Wendt, C. ; Zeppenfeld, D.: Anomalous gauge boson interactions. (1995), Mai, S. 488–547. – ISSN 1793–1339

[9] Evans, Lyndon ; Bryant, Philip: LHC Machine. In: *Journal of Instrumentation* 3 (2008), August, Nr. 08, S. S08001–S08001. `http://dx.doi.org/10.1088/1748-0221/3/08/s08001`. – DOI 10.1088/1748–0221/3/08/s08001. – ISSN 1748–0221

[10] CERN Cooperation: The Large Hadron Collider. Version: 2024. `https://home.cern/science/accelerators/large-hadron-collider`. CERN, 2024

[11] Bianchi, Riccardo Maria and ATLAS Collaboration: *ATLAS experiment schematic or layout illustration*. https://cds.cern.ch/record/2837191. Version: 2022. – General Photo

[12] ATLAS Collaboration: The ATLAS Experiment at the CERN Large Hadron Collider, JINST 3 (2008)

[13] Andricek, L. and others: Das ATLAS Experiment. Version: 2007. https://www.mpg.de/418074/forschungsSchwerpunkt1. Max Planck Gesellschaft, 2007

[14] Krauss, F. ; Greiner, M. ; Soff, G.: Photon and gluon induced processes in relativistic heavy-ion collisions. In: *Progress in Particle and Nuclear Physics* 39 (1997), Januar, S. 503–564. http://dx.doi.org/10.1016/s0146-6410(97)00049-5. – DOI 10.1016/s0146–6410(97)00049–5. – ISSN 0146–6410

[15] ATLAS Collaboration: Measurement of exclusive $\gamma\gamma \rightarrow \ell^+\ell^-$ production in proton–proton collisions at $\sqrt{s} = 7\,\mathrm{TeV}$ with the ATLAS detector. (2015)

[16] Bailey, S. ; Harland-Lang, L. A.: Modelling W^+W^- production with rapidity gaps at the LHC. (2022). http://dx.doi.org/10.48550/ARXIV.2201.08403. – DOI 10.48550/ARXIV.2201.08403

[17] ATLAS Collaboration: Electron reconstruction and identification in the ATLAS experiment using the 2015 and 2016 LHC proton-proton collision data at $\sqrt{s} = 13\,\mathrm{GeV}$. (2019)

[18] ATLAS Collaboration: Muon reconstruction and identification efficiency inATLAS using the full Run 2 pp collision data set $\sqrt{s} = 13\,\mathrm{TeV}$. (2021)

[19] Waldi, Roland: *Statistische Datenanalyse: Grundlagen und Methoden für Physiker*. Springer Berlin Heidelberg, 2019. http://dx.doi.org/10.1007/978-3-662-60645-2. http://dx.doi.org/10.1007/978-3-662-60645-2. – ISBN 9783662606452

[20] Shalaev, V. V. ; Gorbunov, I. N. ; Shmatov, S. V.: Measurement of Angular Coefficients in the Drell–Yan Process in the CMS Experiment at the LHC. In: *Physics of Atomic Nuclei* 84 (2021), Dezember, Nr. 12, S. 2037–2040. http://dx.doi.org/10.1134/s1063778821090313. – DOI 10.1134/s1063778821090313. – ISSN 1562–692X

[21] D'Agostini, G.: A multidimensional unfolding method based on Bayes' theorem. In: *Nuclear Instruments and Methods in Physics Research Section A: Accelerators, Spectrometers, Detectors and Associated Equipment* 362 (1995), August, Nr. 2–3, S. 487–498. http://dx.doi.org/10.1016/0168-9002(95)00274-x. – DOI 10.1016/0168–9002(95)00274–x. – ISSN 0168–9002

[22] D'Agostini, G.: Improved iterative Bayesian unfolding, 2010

[23] ATLAS Collaboration: Measurements of W^+W^- production cross sections in pp collisions at $\sqrt{s} = 13\,\text{TeV}$ with the ATLAS detector, 2023

[24] Gehrmann, T and others: W^+W^- production at hadron colliders in NNLO QCD. (2014). `http://dx.doi.org/10.48550/ARXIV.1408.5243`. – DOI 10.48550/ARXIV.1408.5243

[25] CMS Collaboration: Measurement of the differential Drell-Yan cross section in proton-proton collisions at $\sqrt{s} = 13$ TeV. In: *JHEP 12 (2019) 059* 2019 (2018), Dezember, Nr. 12. `http://dx.doi.org/10.1007/jhep12(2019)061`. – DOI 10.1007/jhep12(2019)061. – ISSN 1029–8479

[26] ATLAS Collaboration: Observation of gauge boson joint-polarisation states in $W^{\pm}Z$ production from pp collisions at $\sqrt{s} = 13\,\text{TeV}$ with the ATLAS detector. (2023)

[27] ATLAS Collaboration: The ATLAS Simulation Infrastructure. (2010)

[28] ATLAS Collaboration: Measurement of the W-boson mass in pp collisions at $\sqrt{s} = 7\,\text{TeV}$ with the ATLAS detector. In: *The European Physical Journal C* 78 (2018), Februar, Nr. 2. `http://dx.doi.org/10.1140/epjc/s10052-017-5475-4`. – DOI 10.1140/epjc/s10052–017–5475–4. – ISSN 1434–6052